33RD CONGRESS
OF THE INTERNATIONAL COUNCIL
OF THE AERONAUTICAL SCIENCES
STOCKHOLM, SWEDEN, 4-9 SEPTEMBER, 2022

ICAS 2022 SWEDEN

# MODEL BASED PERFORMANCE EVALUATION OF AIRCRAFT ACTUATOR TECHNOLOGIES

Felix Larsson[1], Christopher Reichenwallner[2], Alessandro Dell'Amico[1,2] & Petter Krus[2]

[1]Saab AB, SE-581 88, Linköping, Sweden(felix.larsson@liu.se, alessandro.dellamico@saabgroup.com)
[2]Linköping University, SE-581 83, Linköping, Sweden(christopher.reichenwallner@liu.se, petter.krus@liu.se)

## Abstract

This paper intends to demonstrate some of the challenges with selection of technology for aircraft actuation system and ease the selection process through the proposition of a model-based evaluation methodology. This methodology considers comparison of power consumption, power losses and thermal influences on performance and is applied to model and evaluate an EMA, an EHA and an SHA. The models are based on test data from real primary flight control actuators and the results show some fundamental differences in performance, thermal influences and power losses related to operating points of the actuator technologies studied.

**Keywords:** Flight actuators, EHA, EMA, SHA, Electrification

## 1. Introduction

Electrification of aircraft actuators can provide many opportunities such as power on demand capability, removal of hydraulic distribution, ease of maintenance, increased efficiency and in some cases weight savings. However, depending on the required operational domain of the actuator, electrification may be more or less appropriate. Today, the main enabler for electrification is the electric motor, which converts electric power into rotational power within the actuator. Due to their power to weight ratio, and their power/torque characteristics, most often permanent magnet machines, such as the permanent magnet synchronous motor (PMSM), or the brushless dc-motor (BLDC), are used.

Previous research has shown the improvements possible with electrification, where improvements in energy consumption, response, maintainability and environmental factors are some of the main drivers [17] [16] [25]. However, within the limits of the different technologies, the effectiveness of the actuators will differ. Therefore, when analyzing the performance of Electro-Mechanical Actuators (EMA), Servo-Hydraulic Actuators (SHA) and Electro-Hydrostatic Actuators (EHA), it is important to investigate how their attributes change within the full domain of work to fully understand what challenges and opportunities the different technologies bring. An actuator which is used for primary flight control will not only operate in one state, for example max speed, or max force, it will continuously change state throughout the entire flight ranging from low to high performance demands. There is much to read about the different internal components, but presently no full mapping of how the performance correlate to temperature and power consumption for the three different actuator technologies, which make it difficult to understand when a certain technology may be more suitable than another.

This paper intends to present a methodology to analyze the different technologies with respect to energy consumption, temperature and transient power demand. Together with realistic test data from an Iron Bird actuation system test rig, the models can be validated before they are analyzed and compared. The intention is to show the opportunities and challenges with the three different technologies, and provide an indication of when one technology may be more suitable than another with regards to power consumption, temperature and performance.

This analysis will focus on evaluation of real hardware, designed and certified for flight applications. Since the actuators used in this work are not designed to fulfill the same set of requirements, an important and difficult question is raised; - How can we compare systems designed for different purposes? When evaluating existing systems for aircraft, this is a highly important question since all different aircraft types will set different requirements on the systems, implying that there is no unison design. In an early design phase of a new aircraft, if it is known what implications a certain technology for actuation will bring, better decisions can be made.

With regards to modeling of actuators, different actuator architectures and the fundamental differences in between the actuation technologies a lot of information can be found in the thorough work presented in [15], [14], [22] and [21]. In [20], an analytical tool of the sizing process of the internal components of EMAs can be found. A comparison of energy losses in SHAs, EHAs and EMAs during a certain generic flight mission can be found in [23].

## 2. Actuators to be evaluated

In this work, the actuators to be evaluated and compared are an EMA, an EHA and an SHA. At the division of Fluid and Mechatronic Systems (FLUMES) in Linköpings University, physical SHAs and an EMA, both designed as primary flight control actuators, are present in an Iron Bird test-rig. These served as test-objects for model validation within this project.

The EMA utilized in this work consists of a 6-phase, air-cooled dual-redundant PMSM which directly drives a ball-screw. The EMA is supplied and controlled by a separated control box, which both handles power electronics, monitoring and command signals.

The SHA is a dual-redundant, fly by wire actuator which consists of a constant pressure supply, and two fully separated hydraulic cylinders, which are controlled with flapper-nozzle servo valves.

From the knowledge gained by modeling these, a model of a semi-validated EHA was created by reuse of the electric models created for the EMA and some of the hydraulic components for the SHA. A fixed displacement bent-axis pump model to the EHA was created through adoption of a model built in another project within the FLUMES division [19].

## 3. Model-based evaluation methodology

To understand how energy consumption is affected by temperature changes and performance demand for the different energy transformers in the actuator, the power losses must firstly be mapped and analyzed. In figure 1, the power paths of the different actuators are presented. Here, the thermal power is also dependant on the temperature, which creates a snowball effect where more power is lost into heating when the temperature changes. This effect is important to understand since sufficient thermal management system will have to be installed in order to handle the temperature changes.

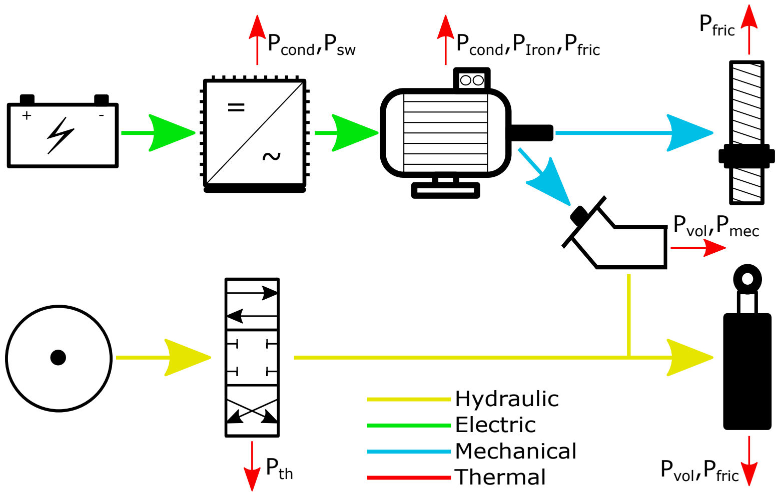


Figure 1 – Overview of EMA EHA and SHA power paths.

In this work, models of the actuators were used to efficiently map the energy consumption throughout the domain of operation. The methodology adopted for creation of the models is presented in figure 2.

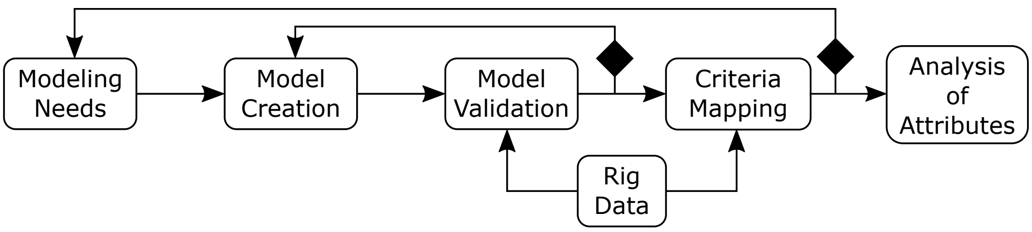


Figure 2 – Overview of the methodology adopted in this work.

First, the modeling needs based on the different criteria to be evaluated was set-up. From this, sufficient models of the actuators internal components were created with Simulink/Simscape predefined components. In some cases where no predefined models met the requirements sufficiently, new components had to be created. The components were then coupled and sized to represent the physical test-objects located in the lab. To control the modeled actuators, controllers were set up based on supplier information.

After this, the models were validated through comparison with simple rig-tests. The intention of this was to verify that the entities to be analyzed behaved similar to the physical actuators when affected to a varying load.

The partly validated models were then used to extract a high number of data points within the operational domain of the actuators, with respect to both static and dynamic operation. With the physical test objects, some different data points could then be extracted to validate the results.

The last step was to analyze the extracted data. Here, all results was normalized, since with normalized values, a relative comparison between the actuators could be done in order to evaluate how the technologies characteristics varied within their operational range, and how they depended on temperature.

## 3.1 Modeling needs

The major focus in this work was to analyze and identify the performance, power consumption and typical characteristics of the actuators within their limitations. Therefor, it was essential to identify the limiting factors of the technologies and create sufficient models which account for the limitations. Table 1 present the model considerations and engineering needs of the models. Here, Y represents yes and N/A means not applicable. This table, and the models created are inspired by the work presented in [15]. Most of the components are represented by standard components in Simulink/Simscape and are sized according to supplier data together with collected data from rig tests.

Table 1 – The model considerations and engineering needs.

| | Engineering needs | | | | | |
|---|---|---|---|---|---|---|
| **Model considerations** | Functional | Power Sizing | Natural Dynamics | Closed-Loop Performance | Consumed Energy | Mechanical Load Propagation |
| **Control** | | | | | | |
| Discrete with saturations | Y | Y | Y | Y | Y | N/A |
| **Electric converters** | | | | | | |
| Intermediate (equivalent DQ, copper losses, inductance, inertia, temperature dependency) | Y | Y | Y | Y | Y | Y |
| **Hydraulic converters** | | | | | | |
| Basic (non-linearities) | Y | Y | Y | Y | Y | Y |
| Advanced (compression, friction) | Y | Y | Y | Y | Y | Y |
| **Mechanical converters** | | | | | | |
| Intermediate (non-linear friction, inertia) | Y | Y | Y | Y | Y | Y |

## 3.2 Model creation

In table 2, the components present in the actuator models and their respective level of model considerations are specified.

Table 2 – The modeled components, their model group and the level of model fidelity.

| | **PMSM** | **Pump** | **Servo valve** | **Ball screw** | **Cylinder** |
|---|---|---|---|---|---|
| **Model group** | Electric converters | Hydraulic converters | Hydraulic converters | Mechanical converters | Hydraulic converters |
| **Model considerations** | Intermediate | Advanced | Basic | Intermediate | Advanced |

Major parts of the EMA- and SHA models used in this work were created during a master thesis project held at the division of Fluid and Mechatronic Systems at Linköping University [18]. These models were then further developed and adapted to suit the needs for the analyzes made in this work.

### *3.2.1 EMA model*

The model of the EMA includes a PMSM which is connected to a ball screw. The PMSM was modeled as a dq-equivalent 6-phase machine to account for saturation in supply power [22] [7]. The model also incorporate rotational friction of the motor bearing and ball screw, which was modeled with respect to both breakaway torque and dynamic torque [8]. Iron losses are difficult to capture in a model and usually quite small in relation to the copper losses, which occur due to the resistance in the stator windings. The iron losses consist of two parts, namely core-losses (eddy and hysteresis losses) and magnetizing losses. During constant power region, the iron losses become significant, while at lower speed/constant torque region, the copper losses are dominant [26] [24].

According to [14], the iron losses can be modeled as a torque loss directly connected to the electric motor axis according to the following equation:

$$T_{ironloss} = \frac{P_{iron}(i_m, \omega_m)}{\omega_m} \tag{1}$$

Where $P_{iron}(i_m, \omega_m)$ is given by the supplier, found from Comutational Fluid Dynamics (CFD) simulations.

The ball screw was modeled as a constant-efficiency lead screw [6] together with rotational friction, rotational inertia and transitional mass. The control scheme of the EMA is presented in figure 3.

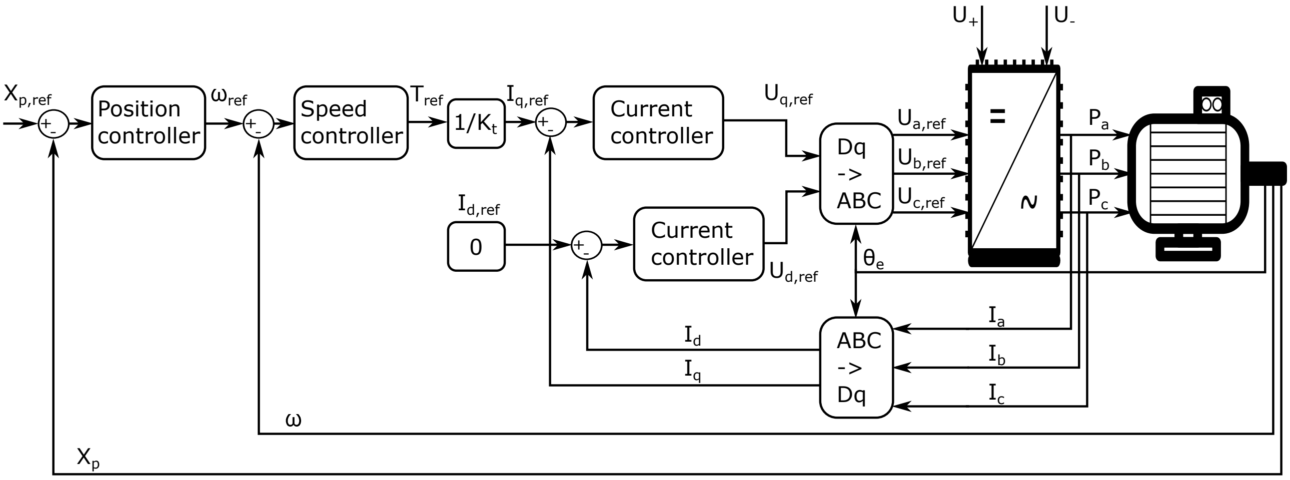


Figure 3 – The control scheme of the PMSM.

Since the focus in this work was not to evaluate control and design of control electronics, the inverter switching dynamics was not included in the model. Instead, the PMSM was directly fed with the altering voltage calculated in the control loop. The inverter was thereby modeled as a equivalent DC circuit to calculate the DC-current required from the EMA through the following equations.

$$I_{DCsupply} = I_{DC,ch1}\alpha_{ch1} + I_{DC,ch2}\alpha_{ch2} + I_{sw,ch1} + I_{sw,ch2} \tag{2}$$

Where $\alpha$ is the actual duty-cycle, which can be calculated from the DC voltage supplied to the electric motor ($V_{DC,ch1,2}$), the DC voltage supply ($V_{DCSupply}$), the switching losses ($I_{sw,ch1,2}$) and the voltage drop over the transistors ($U_{d,ch1,2}$):

$$\alpha_{ch1,2} = \frac{V_{DC,ch1,2} + U_{d,ch1,2}(I_{DC,ch1,2})}{V_{DCSupply}} \tag{3}$$

Where $V_{DC,ch}$ is the equivalent DC-voltage usage per channel which can be calculated with the following equation: [1]

$$V_{DC,ch} = V_{RMS,ch}\frac{2\sqrt{2}}{\sqrt{3}} \tag{4}$$

Where:

$$V_{RMS,ch1,2} = \sqrt{\frac{(V_a - V_b)^2 + (V_b - V_c)^2 + (V_c - V_a)^2}{3}} \tag{5}$$

The equivalent DC current supplied to the motor can now be found through identification.

$$S = 3V_L I_L = \sqrt{3}V_H I_L = \sqrt{3}V_{RMS}I_{RMS} = \frac{3}{2\sqrt{2}}V_{DC}I_{RMS} \rightarrow I_{DC} = \frac{3}{2\sqrt{2}}I_{RMS} \tag{6}$$

Where:

$$I_{RMS,ch1,2} = \sqrt{\frac{I_a^2 + I_b^2 + I_c^2}{3}} \tag{7}$$

In the inverter, there are mainly two types of losses which are important to consider, namely conduction- and switching-losses. [14]

$$U_d = U_{th} + R_{on} I_{RMS} \tag{8}$$

$$I_{sw} = f_{sw} \frac{E_{on} + E_{off}}{U_s} \tag{9}$$

Here, $U_{th}$ is the threshold voltage where the transistors let the power pass, $R_{on}$ represents the on-resistance of the transistors, $E_{on/off}$ is the energy required to switch a transistor, $f_{sw}$ is the switching frequency and $U_s$ is the supply voltage.

It is also important to notice that $R_{on}$, $U_{th}$, $E_{on}$ and $E_{off}$ will change with changed temperature and thereby affect the power consumption of the inverter. However, these effects are not considered in this work.

### 3.2.2 SHA model

The SHA consist of a constant pressure hydraulic supply, two flapper nozzle servo valves and two parallel hydraulic cylinders. The hydraulic servo valves are modeled as flapper nozzle valves, including pilot leakage and under lap. They are modeled by use of variable-area hydraulic orifices [10] from the Simscape library in Simulink. The under lap is modeled as a constant opening span of the servo valve and the pilot leakage is modeled as a constant leakage in between the constant pressure supply and the tank by using a constant area hydraulic orifice [3].

The hydraulic cylinders were modeled by using translational hydro-mechanical converters from the Simscape library in Simulink [9], where two of these were coupled to represent each chamber of the cylinder. Also, an internal cylinder leakage were added by coupling a constant area hydraulic orifice in between the pressure chambers in the cylinder. The two individual cylinders where then coupled to add the output force.

The major losses in an hydraulic cylinder are related to friction and leakage. The friction related losses occur mainly due to friction caused by seals in between translating parts.

$$F_{fr} = f_c L + f_h A, A = \frac{\pi}{4}(d_o^2 - d_i^2), L = d_o \pi \tag{10}$$

Where $f_c$ is the friction per seal contact length, $f_h$ is the friction per seal projected area, $d_o$ is the seal outer diameter and $d_i$ is the seal inner diameter. The term $f_c$ is mainly due to seal squeeze and will thereby be seen as constant throughout the operational domain of the cylinder, while the term $f_h$ will increase due to pressure [11]. The hydraulic cylinder friction is implemented to the model as a pressure dependent friction where the friction due to squeeze represent the pre-load force and the friction due to pressure will be seen as a coulomb friction force [4]. The data used was adapted from data found in [11]. The control scheme of the SHA is presented in figure 4.

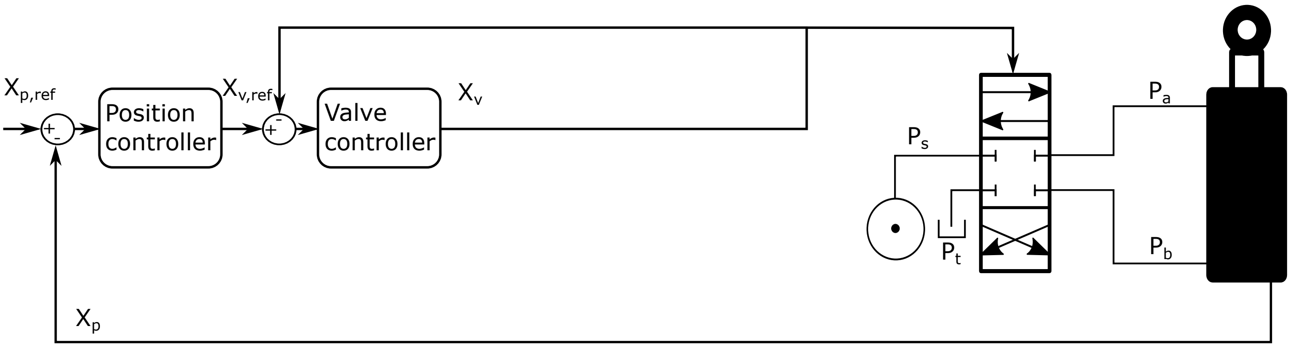


Figure 4 – The control scheme of the SHA.

### 3.2.3 EHA model

The EHA consist of the same components as the EMA, but instead of the ball screw, it incorporate a fixed displacement pump which is connected to a hydraulic cylinder. The hydraulic cylinder was modeled in the same way as for the SHA and was sized to provide similar performance as the EMA. The fixed displacement pump [5] was dimensioned to suit the specification of the electric motor used in the EMA. An efficiency model was adopted from test data presented in [19] to provide the pump behavior. It was assumed that the efficiency map does not drastically change with pump size. However, in this project, it is not the absolute numbers which are interesting, but the differences in characteristics between the technologies. Thereby, it is not highly important that the absolute magnitude of efficiency is found. The total efficiency map (volumetric + hydromechanic) is found in figure 5.

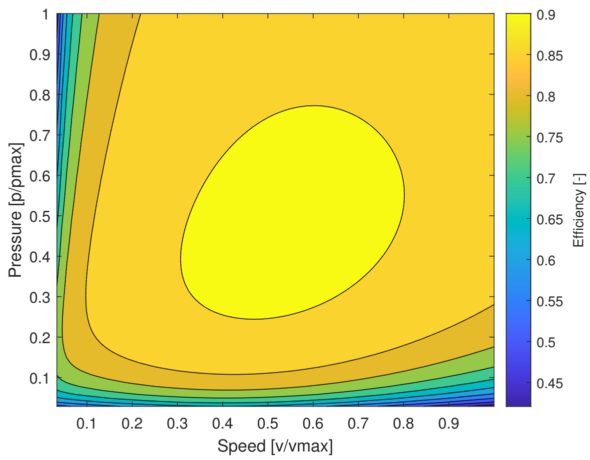


Figure 5 – Efficiency map of bent-axis fixed displacement pump [19].

### 3.2.4 Temperature dependency of models

The variables which will depend on temperature within the scope of this work are:

- Rotor resistance (Copper material properties)
- Viscosity of hydraulic oil
- Electric motor torque constant due to thermal properties of magnets
- Breakaway and dynamic friction of mechanical components
- Efficiency of ball screw

The conduction losses in synchronous machines, such as the PMSM utilized in this work, depends on the resistance in the windings, which cause voltage drop. The windings most often consist of copper wires, which make the resistance dependent on the material properties of copper. These properties change with temperature, causing the resistance to change. This can be described with the following equation:

$$R_{copper} = R_0(1 + \alpha(T - 20)) \tag{11}$$

Where $R_0$ is the resistance of the copper winding at 20℃, T represents the actual temperature of the material and $\alpha$ is the temperature coefficient of resistance, and has the value of 0.00393 0℃$^{-1}$ for copper, according to [13].

The torque constant of the PMSM will decrease with increased temperature. The relative decrease was given by the manufacturer and can be seen in figure 6. This decrease occur due to the reluctance of the magnets and stator are material dependent, and the material properties change with temperature. This will in turn increase the current required to produce the same torque. As previously stated, the rotor resistances will also change with temperature which in turn increase the power losses related to winding resistance. Together with reduced torque constant, a snowball effect is introduced, causing more power losses. Since the maximum motor current is limited, this will eventually decrease the maximum output force of the actuator.

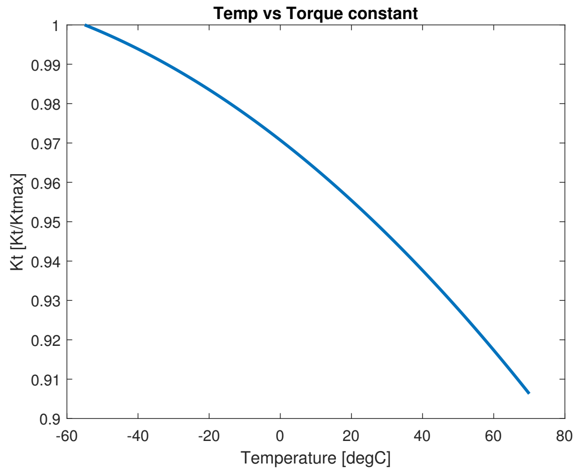


Figure 6 – The relationship between the torque constant (Kt) of the PMSM and temperature.

The friction coefficients of the ball screw are also temperature dependent. With decreased temperature, the friction will increase mainly due to increased viscosity in lubrication. The relationship between friction and temperature is presented in figure 7 and was given by the manufacturer. Here, Tmbor is the motor breakaway and running drag torque, Tbo is the ball screw breakaway torque, Tr is the ball screw running drag torque and etaBsD and etaBsR are the driving- and reverse efficiencies of the ball screw.

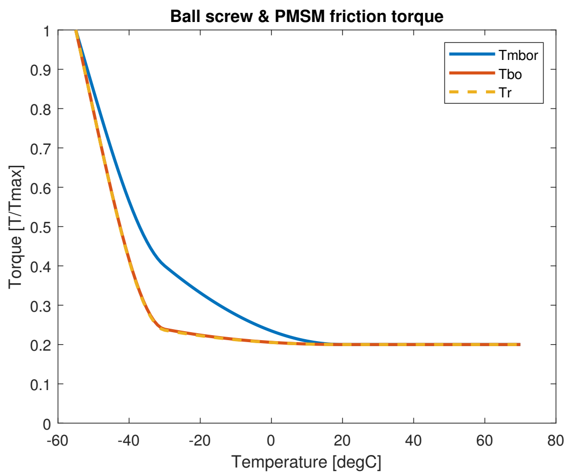


(a) Normalized ball screw and motor breakout- and running drag torque.

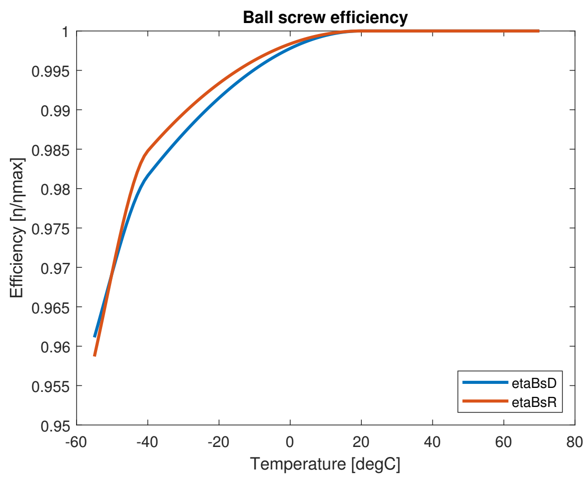


(b) Normalized ball screw efficiency.

Figure 7 – Ball screw- and motor bearing properties related to temperature.

In the hydraulic domain, the losses will be mostly dependent on the flow of oil, causing increased oil temperature, which in turn cause increased leakage. The leakage will increase due to warmer oil will have lower viscosity. However, as long as the required pressure can be achieved by the supply system, the stall-force can be achieved.

When the temperature of the hydraulic fluid changes, its properties such as density, bulk modulus and viscosity, also changes. In the studies which was conducted in this work, the most important property was the viscosity, since it affect the internal and external hydraulic leakage. In figure 8, the viscosity change due to temperature of the flight graded hydraulic fluid Aeroshell 31 is plotted [2]. This curve was interpolated from a low number of data points, which means that in reality, the relationship may be different. However, it provide an indication of how the worst case scenario may affect the performance of the hydraulic actuators.

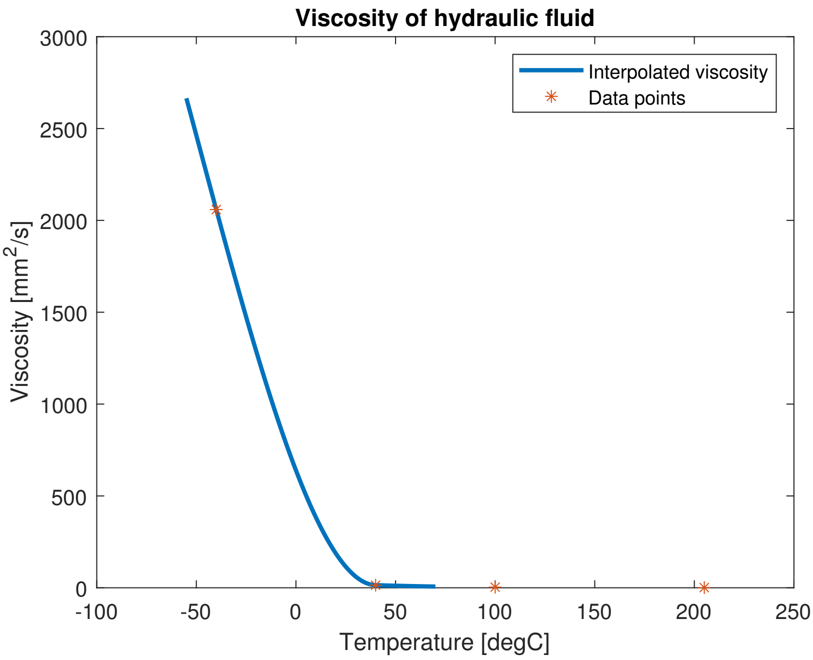


Figure 8 – Viscosity of the hydraulic flight-graded fluid Aeroshell 31.

## 3.3 Model validation

The models were compared against data collected from the Iron Bird test rig in order to validate the trends in terms of power usage. In figure 9, a comparison of the physical and modeled EMA behavior is presented. The physical EMA was subjected to a spring load with varying spring stiffness while it should follow a sinusoidal input position. The subjected force, motor q-current, DC supply current and output position were logged. Then, the same input position and load force were provided to the model to extract the modeled DC current and motor q-current. It can be seen that there are some differences present, but the trends are similar. These results were however determined to be good enough for this work.

## 3.4 Criteria mapping

To evaluate the energy consumption, performance and temperature dependency for the different test objects, three test cases were set up. To understand how the power consumption varies with speed and load force, a quasi-static mapping of the actuators was made. When analyzing how these maps differ in between the actuators, conclusions of which states are most beneficial for the different technologies can be drawn.

However, a quasi static map will not show the dynamic characteristics of the actuators. Since primary flight actuators continuously will respond to demanded or non-demanded change in the aircraft states and, in the case of unstable fighters, act to stabilize the aircraft, it is important to analyze how the different technologies behave with respect to dynamics. Therefor, mapping of how the power consumption of the actuators differ with respect to response was done.

The previously described analyzes was made at a certain set temperature. To understand how the performance of the actuators is affected by changes in temperature, the maximum force and speed (quasi-static) of the actuators were analyzed with respect to temperature changes.

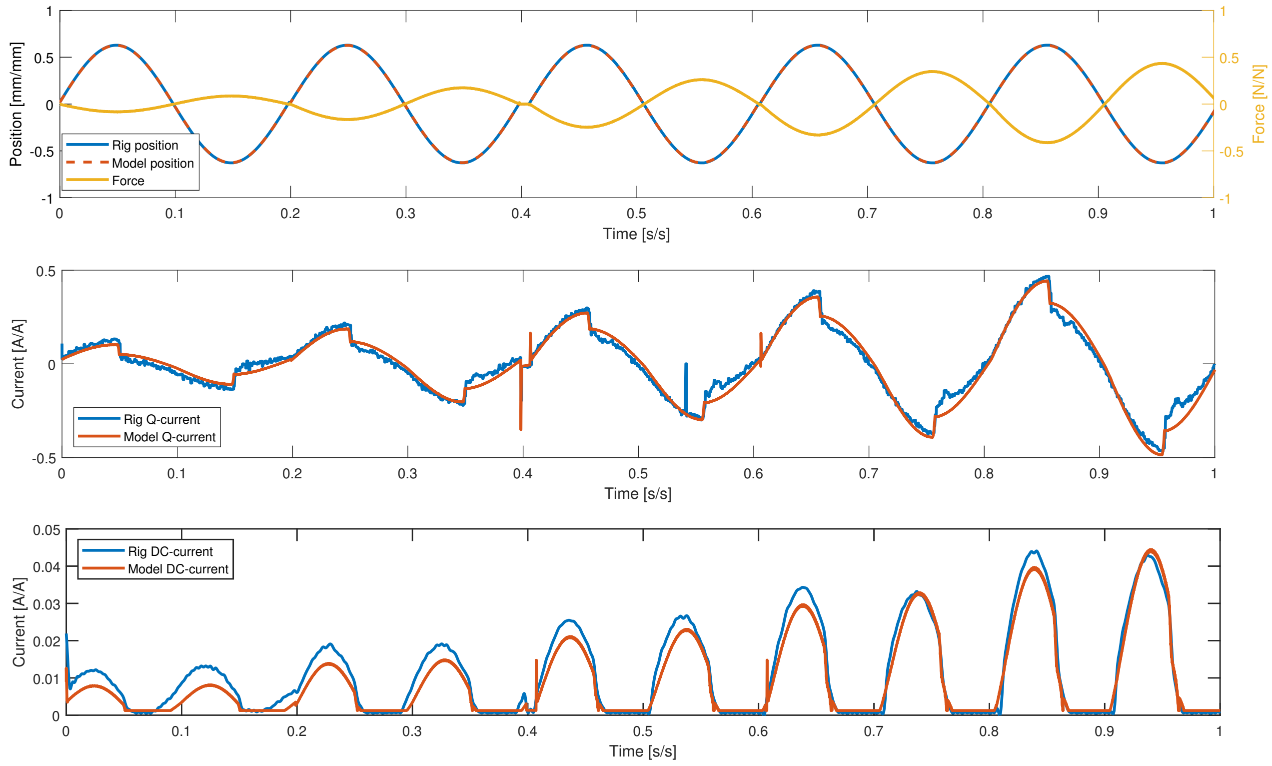


Figure 9 – Validation test for the EMA model.

### 3.4.1 *Quasi-static mapping*

The first case was static mapping, where the correlation between output force and speed was found. Here, a ramp in input position was given to the models. Also, the actuators were affected to a constant load force throughout the test sequence. When quasi-static states (constant speed, zero acceleration) were achieved, data points were extracted. Then, the preconditions (inclination of the input ramp and load force) for the simulation were varied and a new simulation was started. The force and speed were varied from zero up to their maximum values in 21 and 41 steps respectively, which gave a total of 861 data points.

### 3.4.2 *Dynamic mapping*

The dynamic mapping was done by analyzing how the consumed energy depended on frequency response. The actuators were given a sine input as position demand while the energy consumed to perform one period of the sine input was logged. Also, the total distance output during this period was logged. This in order to normalize the energy consumption with respect to distance, since with increased frequency of the sine input the output may differ.

### 3.4.3 *Mapping of temperature influence on performance*

For the mapping of the temperature influence, the actuators were given a large step input in position in order to achieve as much speed as possible. Then, for every new simulation, the force was increased in 41 steps, up to the stall force, i.e. the highest force which can act on the actuator before the load drives it backwards. Similar as for the quasi-static mapping, data were extracted when a constant speed had been achieved by the different actuators. When all force levels had been applied to the actuator, the set temperature was varied which affected the variables previously described and the same procedure was processed. The temperature was varied from minimum to maximum in 6 steps.

## 4. Simulation results

### 4.1 Operational range of actuators

The operational range of the different actuators was found by input a large step in demanded position and analyzing which output speed could be achieved with the current loading. The load was increased from zero until the actuator could no longer output a change in position, i.e. stall was achieved. The implemented limitations in the models were supply pressure, maximum valve opening, supply voltage and maximum current for the SHA and EMA/EHA respectively. The normalized results can be seen in figure 10. Here, the power input and output with respect to actual speed and force can be seen for the different actuators.

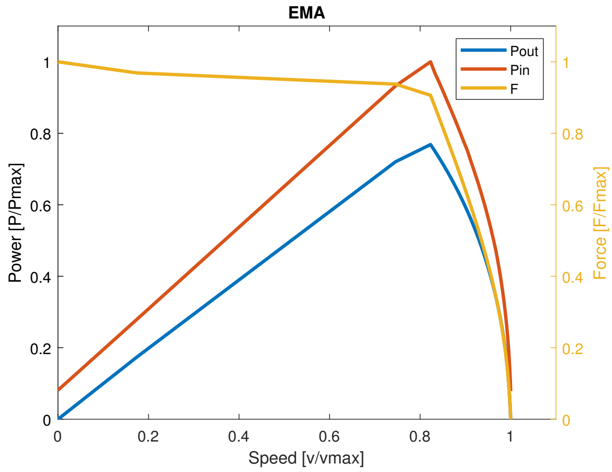


(a) The relationship between speed, force and power for the EMA.

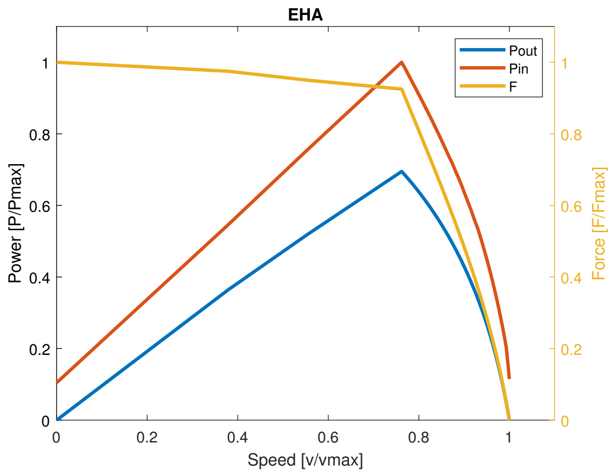


(b) The relationship between speed, force and power for the EHA.

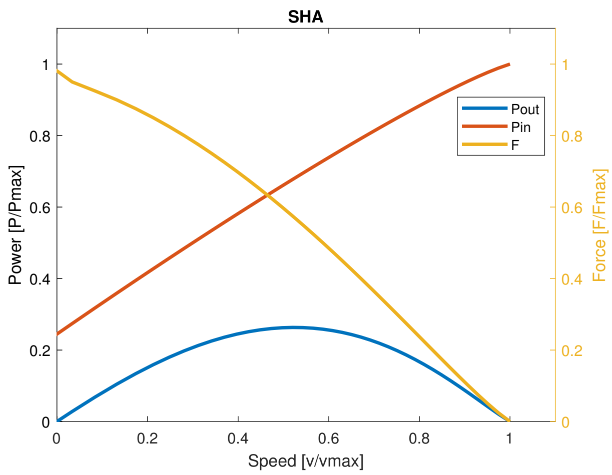


(c) The relationship between speed, force and power for the SHA.

Figure 10 – The relationship between speed, force and power for the actuators.

## 4.2 Quasi-static mapping

The results from this mapping can be found in figure 11. Here, the power loss corresponds to the input power minus the output power, divided with the maximum difference between input and output power, and is represented with the color map.

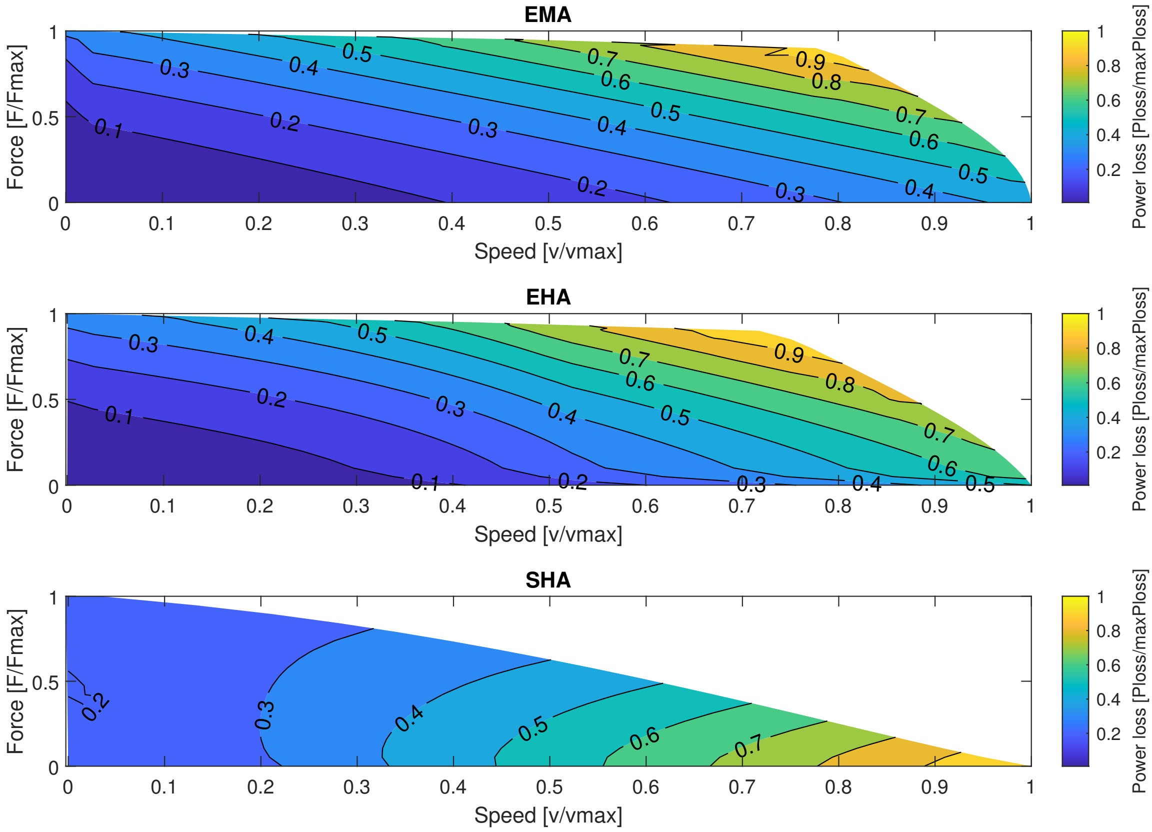


Figure 11 – Correlation between speed, force and power loss.

To fully understand the consequences in running the actuators in different areas within their operational domain, it was found that it is not only important to analyze the power consumption, but also how the loss-driving entities vary. This will show how the losses, and thereby the temperature, propagate related to the different power domains throughout the operational domain. In this case, the power domains which are of interest are electric and hydraulic. Thereby, a second map is presented in figure 12. In this figure, the currents consumed by the electric motor in the EMA and EHA, and the flow to the hydraulic cylinder in the SHA is represented by the color maps.

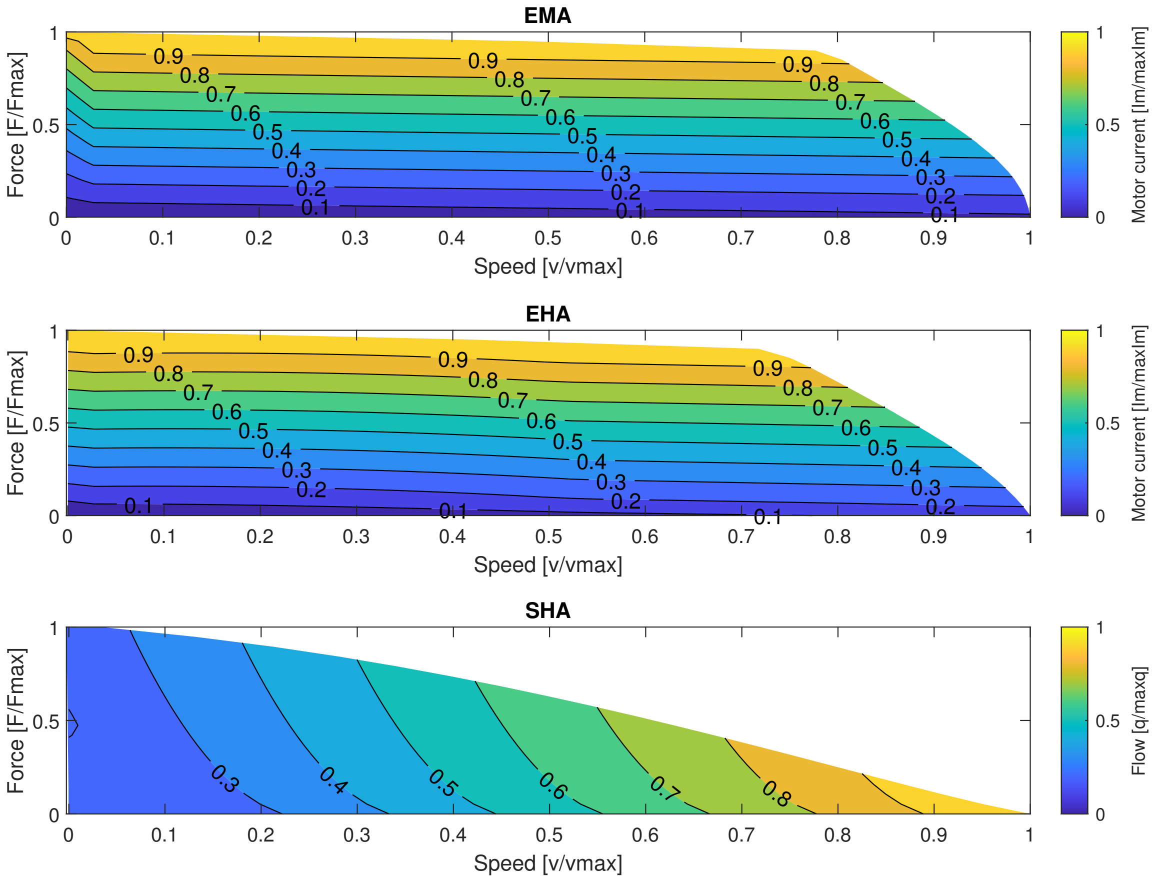


Figure 12 – Correlation between speed, force and motor current/flow

To show how the different components power losses varies within the operational domain, they were plotted in separate figures for four different load levels. In figure 13, the internal power losses in the EMA can be seen. Here, BS correspond to the ball screw, Visc correspond to the viscous friction in the electric motor, Inv is the inverter losses, FricIr is the sum of the rotational friction in the electric motor and the iron losses, and Cu is the copper losses.

In figure 14, the relative power losses of the components in the EHA are presented. Here, Cyl+Pump represents the losses from the hydraulic cylinder and pump, Visc represents the viscous friction in the electric motor, Inv is the inverter losses, FricIr is the sum of the rotational friction in the electric motor and the iron losses, and Cu is the copper losses.

In figure 15, the relative power losses of the components in the SHA are presented. Here, Cyl represents the hydraulic cylinder and SV represent the power losses due to the servo valve. The losses in the servo valve represents both nozzle leakage, leakage due to under lap and the throttling losses.

## 4.3 Dynamic mapping

In figure 16, the results from the dynamic mapping can be seen. It can be seen that the required effort is highly connected to the frequency, or the acceleration of the electrified actuators.
Here, Tot represent the total effort loss required to achieve a certain frequency output, Inv represent the inverter losses, BS is the ball screw, Iner is the inertia, Cu is the copper loss, FrIr is the electric motor friction loss and iron loss, Vi is the viscous friction, Cyl+Pump is the hydro-mechanic losses in the EHA, Regen is the part which could be regenerated with the electrified actuators, Cyl is the cylinder losses and SV is the losses from the servo valve.

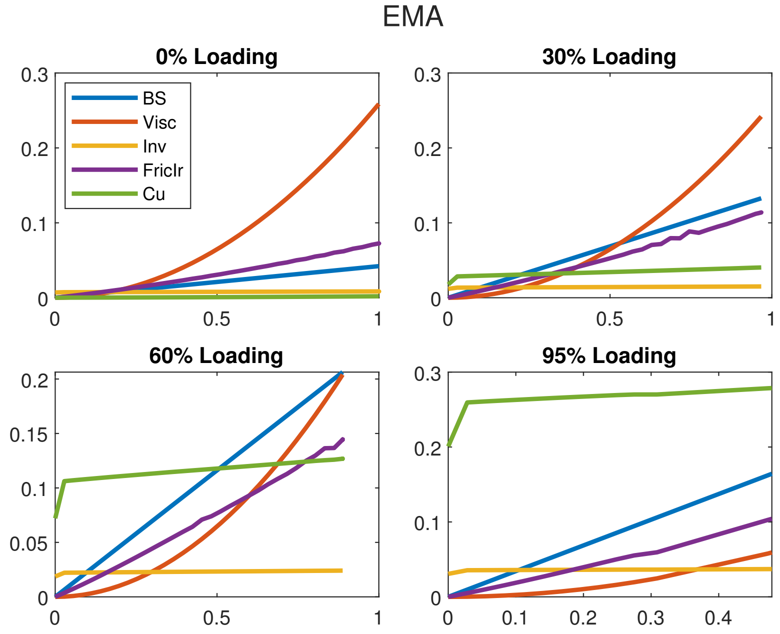


Figure 13 – Losses during quasi-static operation for the EMA.

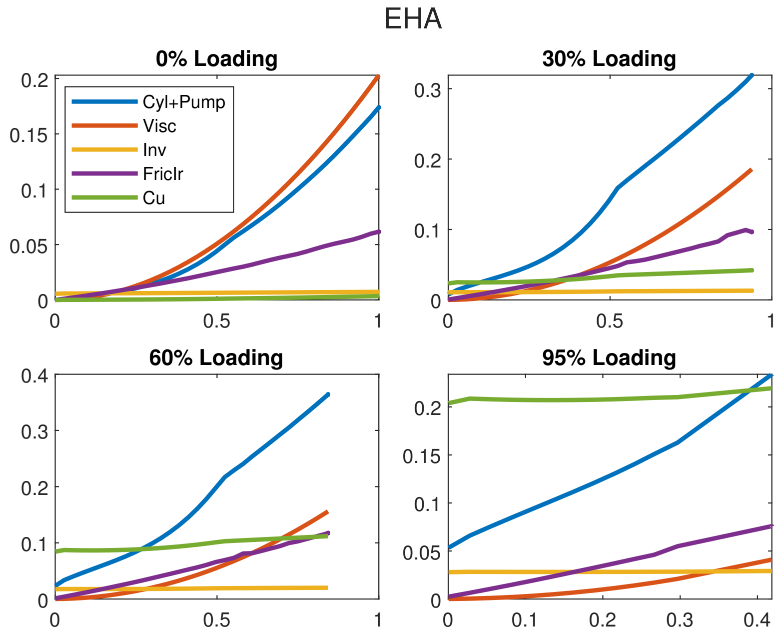


Figure 14 – Losses during quasi-static operation for the EHA.

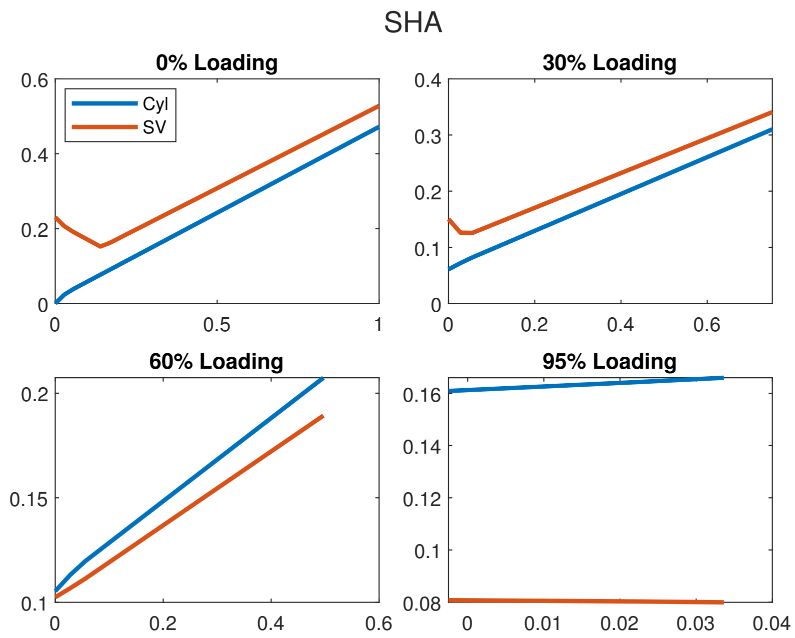


Figure 15 – Losses during quasi-static operation for the SHA.

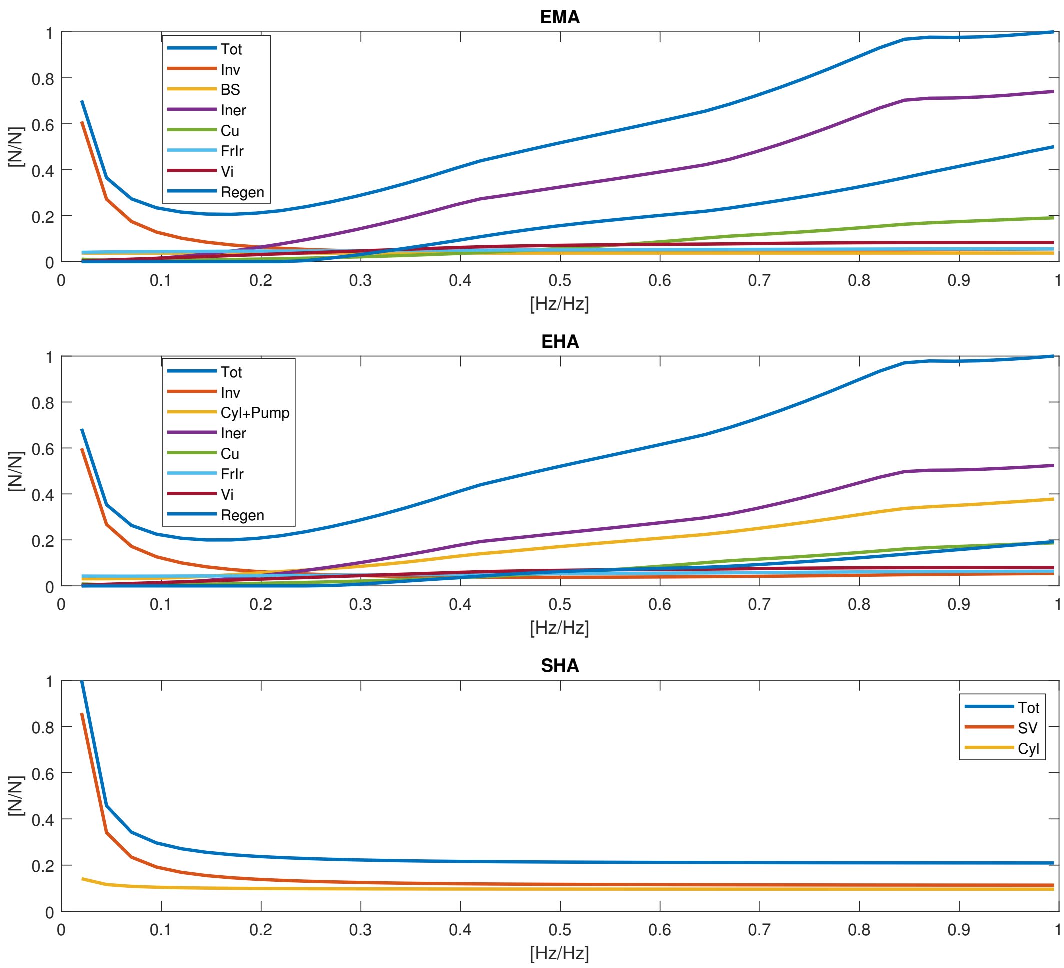


Figure 16 – Dynamic mapping of the required effort related to frequency for the actuators.

### 4.4 Mapping of temperature influence on performance

In figure 17, the quasi-static output force and speed from the EMA with respect to temperature can be seen. It shows that the maximum force is quite constant with temperature increase, while the speed increases with temperature.

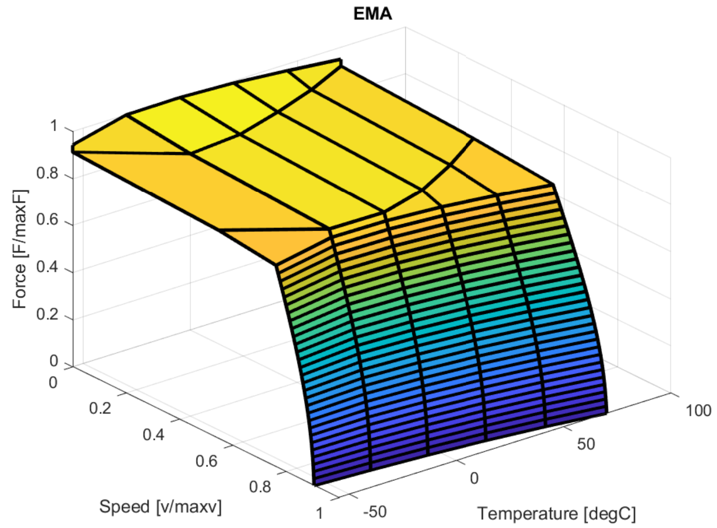


Figure 17 – EMA maximum performance with respect to temperature

In figure 18, the quasi-static output force and speed from the EHA with respect to temperature can be seen. It shows that the maximum force is achieved in cold conditions, while the speed increases with temperature.

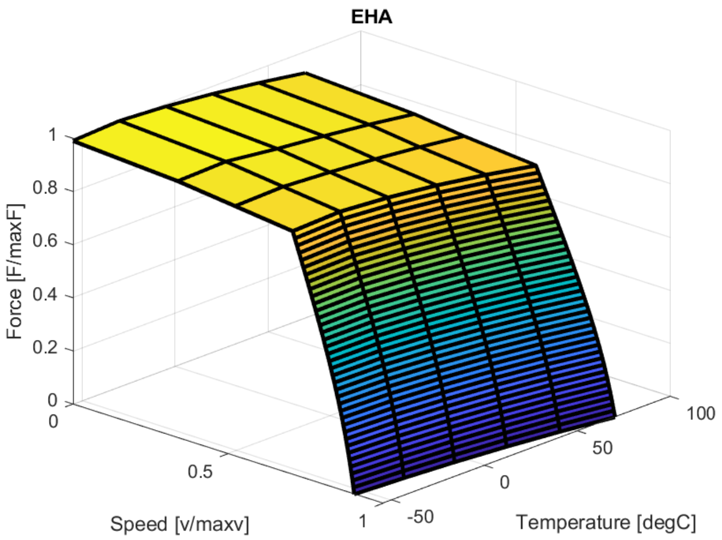


Figure 18 – EHA maximum performance with respect to temperature

In figure 19, the quasi-static output force and speed from the SHA with respect to temperature can be seen. It shows that the maximum speed and force of the SHA is not affected by the temperature.

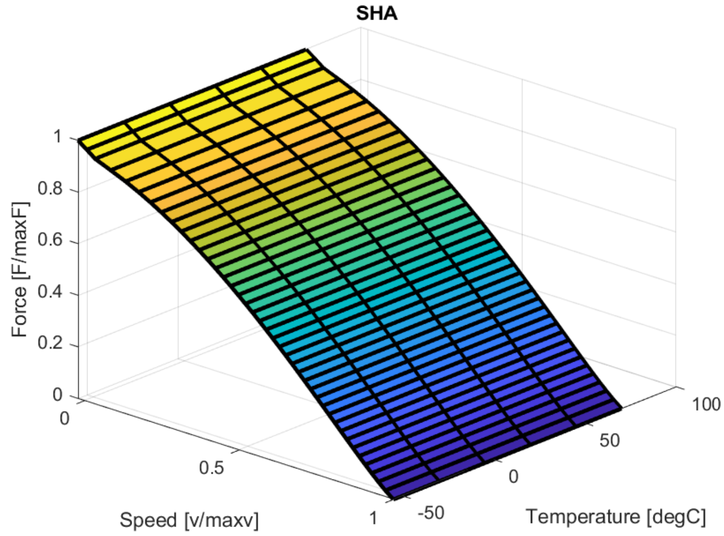


Figure 19 – SHA maximum performance with respect to temperature

## 5. Discussion

### 5.1 Operational range of actuators

As figure 10 show, the difference in input- and output power is lowest for the EMA and highest for the SHA throughout the entire outer operational range. For the SHA, the input power is constantly increasing with speed, while it is more similar to the output power for the electrified actuators. It can also be seen that the operational domain of the different technologies differ quite vastly. The electrified actuators can maintain about 95 % of the maximum load up to about 80 % of the maximum speed, while the force output of the SHA decreases with speed. This is due to the fact that hydraulic flow is a function of pressure difference, while it is a bit more complicated for the electrified actuators. Ideally, the relationship between force and speed should be quite similar as for the SHA, but in this case, saturation is considered. The current which can be demanded by the electric motor is limited to prevent excessive heating of stator windings and transistors in the power electronics. Also, there is a limit to how much flux the magnets can handle. If the current limits would be increased, higher forces may be possible to obtain with the electric motor, which would cause the force and speed relationship to become more similar to the SHA.

### 5.2 Quasi-static mapping

Figure 11 and 12 in combination with figure 10 show that the overall power losses in the electrified actuators are mostly related to the output power, while for the SHA the losses are related to the speed. However, the electric motor in the electrified actuators is highly sensitive to excessive heat. The magnets in the rotor can, in worst case, demagnetize which would cause permanent reduction of available stall force [12]. Also, the stator windings can burn off if the temperature becomes too high where worst case scenario occurs when holding a static load, since then, all current supplied to the motor will float through one winding. The power losses within the electric motor are mostly related to the current fed through the windings, and as can be seen in figure 12, 13 and 14, the motor current is directly related to the load. It is therefore of highest importance to monitor and handle either the load force or the motor currents throughout the flight. However, the relative power losses are much lower for the electrified alternatives, meaning that less power is required from the supply, but it is important to have in mind that the heat generation in the electrified alternatives will be local, while the heat will be transferred with the oil in the SHA. Also, the losses in the SHA are mostly flow related.

Increased force will however increase losses due to leakage and friction in the cylinder, which can be seen figure 15.

### 5.3 Dynamic mapping

In figure 16 it can be seen that there is a correlation between frequency response and effort. For the electrified alternatives, the effort required to accelerate the inertia is the highest contributor. This also cause the copper losses to increase, since current is required to accelerate the inertia. However, a large amount of this could be regenerated by braking the motor by using it as a generator. For the EHA, also the cylinder and pump losses increase with increased frequency. This is due to the fact that the pump also includes extra inertia for the electric motor to accelerate. For the SHA, the effort required decreases with increased frequency. This is since at very low response, a large portion of the flow to the valve leaks to the tank through the under lap. The more the valve is used, the less will leak through the under lap.

### 5.4 Mapping of temperature influence on performance

As can be seen in figure 17, 18 and 19, the electrified alternatives are more sensitive to heat than the SHA. When it comes to the EHA, the influence is mostly related to the magnets in the electric motor, causing the maximum force to increase at cold temperature while the speed is increased when the motor is warm. As can be seen in figure 6, when the rotor is cold, the torque constant will be high, leading to less current is required to produce the same torque. However, as the torque constant is reduced, less back-emf will be generated by the rotor rotation, leading to less voltage is required to produce the same speed. Thereby, at maximum supply voltage, a higher speed can be obtained when the rotor is warm. However, currently the influence of temperature with regards to pump friction is not included in the model, which probably would increase the losses in similar manner as the ball screw. For the EMA, the influences tracks back to both the ball screw and the electric motor. With increased temperature, the ball screw- and motor bearing friction is lowered, as well as the torque constant is lowered, which keep the maximum output force quite constant throughout the temperature range.

### 5.5 General discussion

This approach clearly show the differences in the characteristics of the different actuators and some of the performance-related challenges they give. However, the results are not general for every type of SHA, EMA and EHA. In the case of SHAs, the leakage losses can be vastly reduced by usage of direct-driven servo valves instead of flapper nozzle servo valves. Also, if a load-sensing supply system could be used instead of the constant pressure supply, the throttling losses would be reduced. In the case of the electrified actuators, the set limitations in current greatly affect the characteristics. If, for example, sufficient cooling to handle extreme temperatures would be included, for example water cooling, a higher force possibly could have been achieved. But, with elevated forces the speed would be lowered, which would make the characteristics more similar to the SHA. Also, it is possible to achieve higher speed if the torque constant would be actively controlled through field-weakening. This could provide an opportunity to increase the maximum force of the actuator through increased gear ratio in the ball screw. However, that would put higher stress on the motor during dynamic operation since the acceleration would have to be increased to maintain the same response. Also, there may be physical limitations in at which speeds the ball screw preferably can operate.

The electrified alternatives will provide possibilities to operate with higher speed and force simultaneously than what is possible with a SHA supplied by a constant pressure source. It can be discussed what point of operation which sizes the SHA. If it is the required stall force, or if it is the force which the actuator can handle at a certain speed, can make it more or less interesting to electrify. If the dimensioning case is the latter, the electrified alternative may be more interesting since the SHA would probably have to be oversized. However, if the only interesting points for dimensioning are maximum speed and stall force, regardless of how the relationship in between these points looks like, then the SHA may be preferable.

## 6. Conclusions

This work has shown some of the improvements in actuation performance possible through the usage of electrified actuators. Maybe a certain rudder could utilize SHAs to handle high loads at lower speeds, while another rudder is designed to handle lower loads to higher speeds.

It also show that electrified actuators generally are more effective, where EMA is most effective due to higher the efficiency of the ball screw than the pump. With the information presented in the discussion, it can be stated that a electrified actuator will operate most efficiently when:

- The electric motor is cold
- The ball screw at least intermediately hot
- The acceleration demand is not too high
- The load is low

The SHA will be the most effective when:

- The force is high
- The speed is low

It has been shown that it is possible to draw conclusions and increase understanding of the different actuation technologies through equipment of the proposed methodology. This means that valuable information can be attained through analyzing and comparing physical actuators designed and built to suit different requirement specifications. This can strengthen the need for hardware test rigs equipped with actuators based on different technologies where it should be less difficult to find primary flight actuators designed to fulfill different requirement specifications.

With these results, indications of cooling needs has been shown through the presentation of power losses at different operational points, and the implications in performance of temperature. However, to fully understand how much of an issue heating may be with the different designs, proper thermal models must be included.

## 7. Acknowledgment

The work in this paper was funded by Vinnova, grant number 2017-04888. The authors would like to acknowledge the contribution from the Master Thesis students Johnny Josefsson and Fuad Hanic on the modeling of the EMA and SHA. The authors would also like to thank Saab Surveillance for their support regarding the EMA modeling and testing.

## 8. Contact Author Email Address

Mailto: felix.larsson@liu.se

## 9. Copyright Statement

## References


[1] Average-value inverter (three-phase)). https://se.mathworks.com/help/physmod/sps/ref/averagevalueinverterthreephase.html. Accessed: 2022-04-20.

[2] Aviation hydraulic fluids and preservatives, aeroshell fluid 31 technical data sheet (tds). https://www.shell.com/business-customers/aviation/aeroshell/aeroshell-hydraulic-fluid.html#specs. Accessed: 2022-04-20.

[3] Constant area hydraulic orifice. https://se.mathworks.com/help/physmod/simscape/ref/constantareahydraulicorifice.html. Accessed: 2022-05-27.

[4] Cylinder friction. https://se.mathworks.com/help/physmod/hydro/ref/cylinderfriction.html. Accessed: 2022-05-25.

[5] Fixed-displacement pump. https://se.mathworks.com/help/physmod/hydro/ref/fixeddisplacementpump.html. Accessed: 2022-05-25.

[6] Leadscrew. https://se.mathworks.com/help/physmod/sdl/ref/leadscrew.html. Accessed: 2022-05-25.

[7] Pmsm (six-phase)). https://se.mathworks.com/help/physmod/sps/ref/pmsmsixphase.html. Accessed: 2022-05-25.

[8] Rotational friction. https://se.mathworks.com/help/physmod/simscape/ref/rotationalfriction.html. Accessed: 2022-05-27.

[9] Translational hydro-mechanical converter. https://se.mathworks.com/help/physmod/simscape/ref/translationalhydromechanicalconverter.html. Accessed: 2022-05-27.

[10] Variable area hydraulic orifice. https://se.mathworks.com/help/physmod/simscape/ref/variableareahydraulicorifice.html. Accessed: 2022-05-27.

[11] N K Agarwal and C P Lawson. A practical method to account for seal friction in aircraft hydraulic actuator preliminary design. *Proceedings of the Institution of Mechanical Engineers, Part G, Journal of Aerospace Engineering, Vol 231, Iss 5*, May 2016.

[12] O Bilgin and F A Kazan. The effect of magnet temperature on speed, current and torque in pmsms. *2016 XXII International Conference on Electrical Machines (ICEM)*, September 2016.

[13] J M Eargle. *Resistance Change with Temperature for Copper. In: Electroacoustical Reference Data*. Springer, Boston, MA, 1994.

[14] J Fu, J-C Maré, and Y Fu. Modelling and simulation of flight control electromechanical actuators with special focus on model architecting, multidisciplinary effects and power flows. *Chinese Journal of Aeronautics*, 30(1):47–65, 2017.

[15] J Fu, J-C Maré, L Yu, and Y Fu. Multi-level virtual prototyping of electromechanical actuation system for more electric aircraft. *Chinese Journal of Aeronautics*, 31(5):892–913, 2018.

[16] Li J, Yu Z, Huang Y, and Li Z. A review of electromechanical actuation system for more electric aircraft. Beijing, China, October 2016. IEEE/CSAA International Conference on Aircraft Utility Systems (AUS).

[17] S C Jensen, G D Jenney, B Raymond, and D Dawson. Flight test experience with an electromechanical actuator on the f-18 systems research aircraft. *The 19th Digital Avionics Systems Conference*, October 2000.

[18] J Josefsson and F Hanic. Modeling and real-time simulation of a digital twin for and iron bird flight control system. Master's thesis, 2021. Fluid and Mechatronic Systems, Linköping University.

[19] S Kärnell, A Rankka, Al Dell'Amico, and L Ericson. Digital pumps in speed-controlled systems: an energy study for a loader crane application. *12th International Fluid Power Conference (12. IFK)*, 2020.

[20] A Linderstam. Analytical tool for electromechanical actuators for primary and secondary flight control systems. Master's thesis, 2019. Karlstad University.

[21] J-C Maré. *Aerospace Actuators 2*. ISTE, St George's Road, London, 2017. ISBN 978-1-84821-942-7.

[22] J-C Maré. Practical considerations in the modelling and simulation of electromechanical actuators. *Actuators 2020, MDPI*, September 2020.

[23] J-C Maré and M Budinger. Comparative analysis of energy losses in servo-hydraulic, electro-hydrostatic and electro-mechanical actuators. *11th Scandinavian International Conference on Fluid Power*, 2009.

[24] P H Mellor, R Wrobel, and D Holliday. A computationally efficient iron loss model for brushless ac machines that caters for rated flux and field weakened operation. *2009 IEEE International Electric Machines and Drives Conference*, May 2009.

[25] G Qiao, G Liu, Z Shi, Y Wang, S Ma, and T C Lim. A review of electromechanical actuators for more/all electric aircraft systems. *Journal of Mechanical Engineering Science, Vol. 232, Part C*, 2018.

[26] S D Umans. *Fitzgerald & Kingsley's Electric Machinery, Seventh edition*. McGraw-Hill, New York, 2014.